RSC Advances

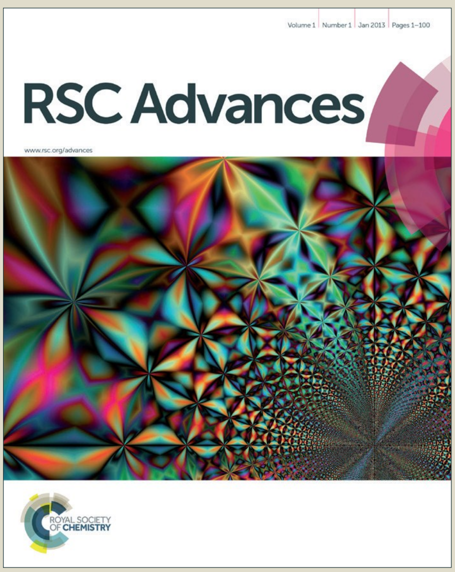

Dehydrochlorination of 1,2-dichloroethane over Ba modified Al_2O_3 catalysts

Shuxing Bai[a], Qiguang Dai[a]*, Xinxin Chu[b], Xingyi Wang[a]*,

Abstract

Bimodal mesoporous alumina (Al_2O_3) was prepared using polyethyleneglycol (PEG 20000) and cetyl trimethyl ammonium bromide as template. The incorporation of Ba with various loadings was carried out by incipient wetness. Characterization was performed by XRD, N_2 sorption isotherms, and pyridine-FT-IR. Ba can be highly dispersed on Al_2O_3 with covering strong acid sites of Al_2O_3. In the catalytic dehydrochlorination of 1,2-dichloroethane (1,2-DCE), the Ba/Al_2O_3 catalysts present high activity, of which Al_2O_3 is most active with 95% conversion at 325 ^oC, related to more Lewis acidic Al^{3+} sites in a tetrahedral environment. 1,2-DCE adsorbs dissociatively on Lewis acid-base pair sites, forming chlorinated ethoxy species, which is supposed to be intermediate species for vinyl chloride (VC) production. At the temperature higher than 400 ^oC, the dehydrochlorination of VC occurs on strong acid sites of Al_2O_3. Ba can promote greatly the selectivity for VC through decrease in strong acid sites. High stable activity for dehydrochlorination and high selectivity for VC can be obtained over Ba/Al_2O_3 in the presence of oxygen.

Keywords: Dichloroethane, alumina, vinyl chloride, Lewis acidity, Ba, dehydrochlorination.

[a] Key Laboratory for Advanced Materials, Research Institute of Industrial Catalysis, East China University of Science and Technology, Shanghai 200237, PR China.

[b] Key Laboratory of Nuclear Radiation and Nuclear Energy Technology, Shanghai Institute of Applied Physics, Chinese Academy of Science, Shanghai 201800, PR China

.

Tel: +86 21 64253183; Fax: +86 21 64253372; E-mail: wangxy@ecust.edu.cn (X. Wang); daiqg@ecust.edu.cn (Q. Dai).

1. Introduction

Vinyl chloride (VC) has been widely used in production of popular homopolymeric and copolymeric plastic materials. The demand for VC as the basic commodity increases greatly with the application of vinyl plastic materials. The production of VC through chemical dehydrochlorination of l,2-dichloroethane (l,2-DCE) has been practiced on a large scale, of which thermal dehydrochlorination of l,2-DCE at 450–500 °C is industrially a main route with 50% conversion and 98–99% selectivity for VC [1,2]. Catalytic dehydrochlorination presented high effective-ness in VC production. Generally, it was considered that the dehydrochlorination of chloroalkanes was promoted by solid base and acid catalysts. Shalygin reported l,2-DCE dehydrochlorination over a series of silicate catalysts, such as Al_2O_3/SiO_2, Ga_2O_3/SiO_2, ZrO_2/SiO_2, BeO/SiO_2 and Y_2O_3/SiO_2, which were acidic solid materials [1]. There were a few reports on the interaction between chloroalkanes and Al_2O_3. Mochida studied the dehydrochlorination of several chloroalkanes (including 1,1,2-trichloroethane, 1,2-dichloropropane and 1,1,2-di-chloropropane) over Al_2O_3, base and acid catalysts under reductive reaction conditions [3]. Dehydrochlorination reactions over dry Al_2O_3 were postulated to proceed through an E2-concerted mechanism, where the chlorine and hydrogen were eliminated almost simultaneously with the basic and acid sites of Al_2O_3. Feijen-Jeurissen [4] reported that the mechanism of catalytic decomposition of 1,2-DCE over γ-Al_2O_3, and proposed that the destruction of 1,2-DCE occurs through dehydrochlorination to VC. Catalytic cracking of EDC is also practiced industrially over silicates, metal promoted aluminas, or zeolites, but the advantage balance the drawback of needing catalyst regeneration. The dehydrochlorination of chlorided linear paraffins to linear olefins in the production of alkylbenzene sulfonate surfactants was performed catalytically in the presence of silica-aluminas or on metal packings of reactor columns acting as catalysts. In this case, no information is readily available in the open literature concerning catalyst stability.

Recently, transitional alumina has been among the most used materials in any field of technologies, while details of their physicochemical properties are still a matter of discussion and investigation [5]. The crystal structure of γ-Al_2O_3 was still a matter of controversy, being a defective non-stoichiometric spinel [6,7] or other cubic or tetragonal structures with the occupancy of non-spinel cationic sites [8-11]. Digne et al. [12,13] reported DFT results that the two main orientations (under practical operation conditions) of γ-Al_2O_3 facets were <100> (17%) and <110> (70%). The <100> facets were fully dehydrated at 600 K, leading to the formation of coordinatively unsaturated (penta-coordinate) Al^{3+}. As reported, the acidity of γ-Al_2O_3 was related to coordination degree of Al^{3+} species, of which, the strongest Lewis acid sites were associated with very low coordination Al cations, such as tri- and tetra-coordinated Al^{3+}. In the dehydration of ethanol, the most active sites were believed to be Lewis acidic Al^{3+} sites in a tetrahedral environment located on the edges and corners of the nanocrystals [14]. In this paper, the surface structure of Al_2O_3 was modified with dropping Ba, and the effect of the corresponding acidity of Al_2O_3 on the activity, selectivity and stability in the catalytic dehydrochlorination of l,2-DCE were investigated. TPSR and *in situ* DRIFTS techniques were utilized to determine reaction intermediates and thus explore a possible reaction mechanism.

2. Experimental

2.1. Catalysts Preparation

Bimodal mesoporous alumina (Al_2O_3) was synthesized using polyethylene-glycol (PEG 20, 000) and cetyl trimethyl ammonium bromide (CTAB) as template. The typical procedure was described in Ref [15]. CTAB (1.38 g), PEG (2.25 g) and aluminium isopropoxide ($Al(O\text{-}i\text{-}Pr)_3$ 5 g) were dissolved in ethanol aqueous solution (63% V/V) with stirring vigorously, and then ammonia (19 ml) as a precipitation agent was added and stirred for 30 min at 50 ^{o}C. The produced suspension was aged at 50 ^{o}C for 24 h under static conditions. The obtained filter was washed with ethanol and dried at 110 ^{o}C overnight. Dried samples were calcined for 3 h at 550 ^{o}C in air. Commercial Al_2O_3 (Al_2O_3-C) was referred to as a reference.

A series of Ba/Al_2O_3 catalysts with various Ba loadings were prepared by conventional impregnation methods described elsewhere [9]. The support Al_2O_3 (2 g) was impregnated with an aqueous solution (4 ml) (the content of barium nitrate is in a range of 0.0048-0.095 g mL^{-1} (0.05-10 wt%)) and then dried at 80 ^{o}C for 12 h and calcined in air at 550 ^{o}C for 3 h. The obtained catalysts were noted as xBa/Al_2O_3 where x presents the content of Ba wt%. Al_2O_3 used in this work is the bimodal mesoporous Al_2O_3 as unless stated otherwise.

2.2. Catalyst characterization

The powder X-ray diffraction patterns (XRD) of samples were recorded on a Rigaku D/Max-rC powder diffractometer using Cu Kα radiation (40 kV and 100 mA). The diffractograms were recorded within the 2θ range of 10−80 ° with a 2θ step of 0.01 ° and a time step of 10 s. The nitrogen adsorption and desorption isotherms were measured at 77 K on a Micromeritics ASAP 2400 system operated in static measurement mode. Samples were outgassed at 350 °C for 4 h before the measurement. The specific surface area was calculated by using the BET model. The actual Ba contents were determined by inductively coupled plasma atomic emission spectrometry (ICP-AES) using a Varian 710 spectrometer. Samples were dissolved by using aqua regia-hydrogen peroxide system to form a homogeneous solution. The X-ray photoelectron spectroscopy (XPS) measurements were made on a VG ESCALAB MK II spectrometer by using Mg K_α (1253.6 eV) radiation as the excitation source. Charging of samples was corrected by setting the binding energy of adventitious carbon (C1s) at 284.6 eV. The powder samples were pressed into self-supporting disks, loaded into a sub-chamber, which was evacuated for 4 h prior to the measurements at 298 K. Temperature programmed surface reaction (TPSR) measurement was carried out under the condition same as in catalytic activity tests. First, the feed containing 1,000 ppm 1,2-DCE and Ar balance flowed continuously over the samples at 100 °C. After the adsorption-desorption reached an equilibrium, the samples were heated from 100 °C to a specified temperature at the heating rate of 10 °C/min. The reactant and the products (such as DCE (m/z=98), CO_2 (44), CO or C_2H_4 (28), ^+CHO (29), Cl_2 (70), HCl (36), C_2H_2 (26), C_2H_3Cl (62), C4 (41,

CH_2=CH-CH_2^+)) were analyzed on-line over a mass spectrometer apparatus (HIDEN, QIC-20).

2.3. Catalytic activity measurements

Catalytic dehydrochlorination was carried out at atmospheric pressure in a continuous flow micro-reactor (a quartz tube of 3 mm inner diameter). 75 mg catalyst (grain size, 40-60 mesh) was packed in the reactor bed. Before testing the activity and selectivity, the transport effects were investigated to ensure that experimental results were not significantly influenced by interphase transportation. Calculation of the theoretical external transfer rate of reactants to the catalytic particles (at a typical temperature 300 ^oC) based on estimated mass-transfer coefficients gave a value magnitude three orders greater than the measured reaction rates, indicating process conditions were far from external diffusional limitations. The effects of external mass-transfer resistances were experimentally evaluated by repeating a set of process conditions whilst employing a different linear velocity. Results of these experiments indicated that conversion was not affected for linear velocity higher than 7 cm s^{-1}, within the experimental error. Likewise, estimates of interphase temperature gradients showed fluid-solid differences of less than 1 ^oC. The possibility of internal pore diffusion was examined by measuring conversions at fixed conditions but varying catalyst particle size. Results showed that pore diffusional resistance was absent for particles less than 1 mm in diameter. Intraparticle mass-transfer resistances were theoretically evaluated by computing effectiveness factors, which were calculated to be greater than 0.98, indicating that intraparticle mass-transfer resistances were not significant. Finally, internal thermal gradients also proved to be negligible over the range of conditions evaluated in this study. The feed flow through the reactor was set at 40 ml/min (linear velocity of 9.4 cm/s) and the gas hourly space velocity (GHSV) was maintained at 30,000 h^{-1}. Feed stream to the reactor was prepared by delivering liquid 1,2-DCE with a syringe pump into dry Ar and the injection position was electrically heated to ensure complete evaporation of the liquid reaction feeds. The temperature of the reactor was measured with a thermocouple located just at the bottom of the micro-reactor. The effluent gases were analyzed on-line at a given temperature by using gas chromatographs (GC9790, FULI) equipped with a Kromat-KB-5-30 m × 0.32 mm × 0.50 μm capillary column and a flame ionization detector (FID) for the quantitative analysis of the organic chlorinated reactant. Catalytic activity was measured over the range 150−450 °C and the conversions were calculated by subtracting the outlet concentration from the inlet concentration of the reactant and dividing by the inlet concentration. These conversions were obtained at different temperatures under steady state at each temperature. All the reactions were repeated three times to assure reproducibility. Furthermore, carbon balances could be as accurate as within 5%.

2.4. In situ FTIR

In situ diffuse reflectance infrared Fourier transform spectroscopy (DRIFTS) experiments were conducted on a Nicolet 6700 FTIR fitted with a liquid nitrogen cooled mercury-cadmium-telluride detector (MCT). The DRIFTS cell (Harrick, HVC-DRP) fitted with ZnSe windows was used as the reaction chamber that allowed samples to be heated to 550 ^oC. All the spectra were obtained averaging 64 scans. Considering the instrumental optics and the strong framework adsorption of alumina, the useful spectral range was: 4000-1100 cm^{-1}. Prior to 1,2-DCE adsorption experiments, the samples were pretreated in Ar at 550 ^oC for 2 h. Then the samples were cooled down to 50 ^oC in order to remove the contaminants. The spectra of the samples (20-30 mg) were recorded from 100 to 400 ^oC after 1,2-DCE adsorption following sweeping with Ar.

3. Results and discussions

3.1 Catalyst Characterization

3.1.1 Physic properties

Fig. 1 shows N_2 sorption isotherms of samples with the insert of pore size distribution determined based on the adsorption branch using the BJH method. The synthesized Al_2O_3 presents two continuous type-IV curves with a H1-type hysteresis loop, which locates at relative pressure of 0.4-0.55 and 0.55-0.95, respectively. There appear two kinds of pores with radios of 3.9 and 7.4 nm in the pore distribution curve, respectively. BET area is estimated to be 330 m^2/g (Table 1). With the incorporation of Ba into Al_2O_3 by 1~2 wt%, similar N_2 sorption isotherms are observed. Further increase in Ba loading makes two kinds of pores decrease to 3.7 and 5.0 nm, respectively. BET areas of Ba/Al_2O_3 samples are in a range of 310~334 m^2/g (Table 1). Commercial Al_2O_3 (Al_2O_3-C) has a narrow pore size distribution centered at 6.1 nm with surface area of 117.9 m^2/g. XRD patterns of samples are presented in Fig. 2. All of samples exhibit diffraction peaks at 19.4, 37.6, 45.8 and 67.0 °, ascribed to

<111>, <311>, <400> and <440> planes of γ-Al_2O_3, respectively (JCPDS 10-0425). Note that no diffraction peaks due to Ba species are detected for Ba/Al_2O_3 samples with ≤3 wt% Ba loading, implying that Ba species are highly dispersed on surface of the Al_2O_3. With further increase in Ba loading up to 4 wt% or higher, there appear new diffraction peaks at 23.9, 24.3, 33.7, 34.1, 34.6 and 42.0 °, which can be resulted from $BaCO_3$ crystalline phase (JCPDS Card No. 05-0378). The formation of $BaCO_3$ should be related to the interaction of BaO with CO_2 during the calcinations due to strong basicity of BaO.

Fig. 3 shows HRTEM images of the synthesized Al_2O_3 and 4Ba/Al_2O_3 samples. With the presence of Ba, no evident change in morphology is observed. The size of observed Al_2O_3 particles is in a range of 3-7 nm (white circles in Fig. 2A). The small Al_2O_3 particles were stacked together to form a large plane. The lattice spacing was measured to be 0.14 and 0.20 nm, in good agreement with those of the <440> and <400> crystal planes of the standard γ-Al_2O_3 sample (JCPDS 10-0425). The observation of electron diffraction rings in the selected area electron diffraction (SAED) patterns (insets of Fig. 3A) suggests the formation of a polycrystalline structure. The images also show that the catalysts are homogeneous with the absence of crystalline Ba oxide or $BaCO_3$ phases. To further characterize the distribution of Ba in 4Ba/Al_2O_3, the STEM mapping of Ba, Al and O was conducted. As shown in Fig. S1, Ba species were uniformly and highly dispersed on the Al_2O_3 surface. This result shows the strong interaction between Ba and Al_2O_3, as reported elsewhere [9,16,17]. A low BaO coverage of 2 wt% on γ-Al_2O_3 monomeric BaO units were present almost exclusively and these molecularly dispersed BaO units were concentrated on the (100) faces of the alumina crystallites [9]. Density functional theory calculations predicted that energetically most favorable BaO monomer and dimer units anchor to penta-coordinate Al^{3+} sites on the (100) faces of γ-Al_2O_3 in such geometries that maximize their interactions with the support surface [16]. In our case, Al_2O_3 exposed mainly <400>, which is really different from the above results [9,16]. BaO monomer and dimer units should be formed because the aggregation of BaO can not be observed on 4Ba/Al_2O_3 where Ba species is highly dispersed on Al_2O_3 (confirmed by HRTEM). Additionally, the crystalline particles of $BaCO_3$ are not detected by HRTEM, indicating that XRD diffraction from $BaCO_3$ may be due to a separate phase from Al_2O_3 produced during calcinations.

3.1.2 Pyridine adsorption

Pyridine, as a basic probe molecule, can be used for characterization of catalyst surfaces, allowing also a definite determination of the existence of Lewis acidity. The spectra recorded after adsorption of pyridine on Ba/Al_2O_3 samples are presented in Fig. 4. On Py-FT-IR spectra, the typical features of Lewis bonded pyridine can be observed. Over Al_2O_3, three 8a components observed at 1574-92, 1612 and 1624 cm^{-1} reveal the existence of at least three different families of Lewis acid sites, as discussed previously for transitional alumina [5,18-22]. The typical assignments for the first and the last of these three components are to pyridine bonded to octahedral and tetrahedral Al^{3+} ions, respectively, both with a single coordinative unsaturation, thus being penta- and tri- coordinated, respectively, before pyridine adsorption. The band in the middle can be resulted from pyridine species interacting either with Al^{3+} ions in coordination five or to sites having Lewis acid strength slightly lower than tri-coordinated Al^{3+} ions. These sites may be tri-coordinated too, but with a nearest cation vacancy. The spectra observed on the samples containing Ba are very similar, as also are most spectra reported in the literature for pyridine adsorbed on aluminas [23]. As previously reported, the penta-coordinate aluminum ions on γ-Al_2O_3 were identified as the preferential anchoring points for Ba [16] and Pt [17]. It should be noted that with an increase in Ba loading, the intensity of the band at 1624 cm^{-1} decreases gradually and the 8a band at 1574-92 cm^{-1} becomes weaker and narrower. This is possibly due to the coverage of Ba species on tri- and penta-coordinated Al^{3+} ions, thus leading to a decrease in pyridine molecule adsorbed on these sites. In the spectrum of commercial Al_2O_3-C, the features of pyridine adsorbed on Lewis sites are also evident. However, the band at 1612 cm^{-1} due to pyridine species interacting either with Al ions in coordination five becomes significantly strong, while the bands due to tri-coordinated Al^{3+} species, weak, indicating that the number of strong Lewis acid sites on Al_2O_3-C is smaller than Al_2O_3 and Ba/Al_2O_3 with low Ba loading.

3.1.3 NH_3-TPD analyses

Fig. 5 shows NH_3-TPD profiles of Al_2O_3 and Ba/Al_2O_3 samples. NH_3-TPD profiles can be divided into two desorption temperature ranges of 150~300 ^{o}C and 300~450 ^{o}C, corresponding to ammonia desorption from weak and strong acidic sites, respectively. The weak and strong acid amounts of sample with 1% Ba increase by 8% and 23% compared with those of Al_2O_3, respectively (in Table 1). As mentioned previously, the addition of Ba will create an interface between Al-O and Ba-O species which distorts the surface structure of γ-Al_2O_3, probably with electronic unbalance due to the change in length of Al-O bonds, which can contribute the increase in acidity. Further increase in Ba loading, however, both strong and weak acids decrease significantly. Additionally, BaO is a base solid, and it is expected that the acid amount decreases with the formation of BaO particles over Al_2O_3. Thus, for the samples with Ba loading of higher than 4%, the total acidity is inversely proportional to Ba content (Fig. 5 insert). On Py-FTIR spectra of all samples, there appear characteristic peaks of pyridine adsorbed on Lewis acid sites at ca. 1442, 1574-92, 1612 and 1624 cm^{-1} (Fig. 4) [19]. Obviously, Al^{3+} ions coordinated with different number and Ba^{2+} ions for the samples with low Ba content contribute to Lewis acid sites.

3.2 Dehydrochlorination

3.2.1 Activity test

The total conversions of 1,2-DCE over Al_2O_3 and Ba/Al_2O_3 catalysts in dry feed of 1000 ppm 1,2-DCE and Ar balance as functions of temperature are shown in Fig. 6. Al_2O_3 presents considerably high activity and the conversion of 1,2-DCE increases quickly with raising temperature. $T_{95\%}$ (the temperature needed for 95% conversion of 1,2-DCE) is 325 ^{o}C. Main products are composed of VC, aldehyde, ethyne and C_4 (butene or chloro-butene) (Fig. 6), which are confirmed by TPSR (Fig. S2.). C_4 appears only at high temperature with low selectivity (below 1%). The selectivity for VC is promoted by raising temperature with a significant decrease in aldehyde content and reaches 95% at 350 ^{o}C. After that, the selectivity for VC decreases quickly, and is only 60% at 425 °C. Generally, it is considered that the formation of VC is through the dehydrochlorination of 1,2-DCE [4]. Cl atom of 1,2-DCE adsorbs on the Al^{3+} acidic site and surface O^{2-} species or hydroxyl group from the surface of γ-Al_2O_3 nucleophlically attacks the carbon atom of 1,2-DCE and the dehydrochlorination occurs. The formation of aldehyde was considered to be the results of the reaction of VC with surface hydroxyl group over acidic catalysts [24]. As the reaction proceeds with the increase in temperature, the surface oxygen species become less and less, and the formation of aldehyde becomes difficult. At the temperature of 375 °C or higher, VC can be further dehydrochlorinated into ethyne.

With incorporation of Ba, the conversion curve shifts to high temperature. $T_{95\%}$ is proportional to Ba loading (Table 1) and increases from 350 °C for Al_2O_3 to 471 °C for 10Ba/Al_2O_3, indicating that the activity is inhibited by Ba to some extent. Similar product distribution over catalysts containing Ba is available. However, aldehyde distribution become broader and higher with an increase in Ba loading and the selectivity for aldehyde over 4Ba/Al_2O_3 reaches 60% at 225 °C. In all case, the higher the 1,2-DCE conversion, the higher the VC selectivity; the lower the DCE conversion, the higher the aldehyde selectivity. At complete conversion, aldehyde is not formed at all, suggesting that 1,2-DCE partial pressure available is a key factor favoring aldehyde (at low conversion, with more aldehyde available) or VC (at high conversion). In fact, the dependence of the aldehyde formation is expected to have a higher reaction order with respect to 1,2-DCE than VC synthesis. On the other hand, the presence of Ba can produce additional oxygen species as strong basic sites, and so be favorable for the formation of aldehyde through nucleophilic attack (see later). Moreover, the formation of ethyne during increasing temperature decreases gradually with Ba addition. At 425 ^{o}C, the selectivity for ethyne decreases from 60% over Al_2O_3 to 5% over $4Ba/Al_2O_3$. The elimination of HCl from chloroalkanes is promoted by solid base and acid catalysts. Generally, the reactivity of the chlorinated ethylenes decreases with increasing chlorine content in the molecule. The rate determining step probably does not involve breaking the C–Cl or C–H bonds. Bond et al. [25] suggested that over a Pt/Al_2O_3 catalyst, the rate determining step is the removal of chlorine atom. Chintawar et al. extensively studied the oxidation of chlorinated ethylenes [26]. They found a strong correlation between the adsorption capacity of the molecule on the catalyst and the reactivity of the molecule. The elimination reactions of the chlorocompounds over Al_2O_3 in dry feed were postulated to proceed through an E2-concerted mechanism where the chlorine and proton were eliminated almost simultaneously by the acidic and basic sites of Al_2O_3. If the acidity of the proton was weak enough, such as that in the case of VC, the removal of Cl atom on strong acid sites was critical. At that time, the elimination may proceed via E1-concerted mechanism. For Ba/Al_2O_3 catalysts, the decrease in strong acid sites is really not favorable for the activation of VC, even though the basicity of Ba/Al_2O_3 catalysts is strong. As expected, Al_2O_3-C with less strong acidity shows a poor selectivity for ethyne at high temperature. Al_2O_3-C with less strong basic sites (basic oxygen species as BaO possesses) presents lower selectivity for aldehyde.

In order to investigate the effect of acidity on catalysts on the kinetics of

1,2-DCE dehydrochlorination, TOF based on the mole number of converted 1,2-DCE molecules per second per mole of acidic site on the surface of catalysts can be used for comparing activity difference among the acidic sites of Al_2O_3 and Ba/Al_2O_3. Fig. 6 insert shows the TOF at 300 ^oC as a function of Ba loading. It can be seen that the TOF decreases almost linearly with Ba loading. A few studies have been published on the interaction between chloroethanes and Al_2O_3. A significant difference in TOF indicates that a rate determining step probably does not involve breaking C–Cl bonds. The removal of Cl species from the surface may be a slow step [27].

3.2.2 The stability

Considering possible effects of Cl and carbon depositions on the surface of catalysts, the stability tests in the feed of 1000 ppm 1,2-DCE and Ar balance were carried out at 400 ^oC and the results are shown in Fig. 9. It can be seen that the conversion on Al_2O_3 and 4Ba/Al_2O_3 decrease by 50% on stream within first 45 and 18 h, respectively. The used catalysts in stability test became black. EDS analyses showed that there was 1.5~2.7% carbon deposition. This phenomenon implies that the polymerization, fuse and carbonization can occur during reaction. Moreover, about 2% Cl was detected by XPS and EDS analyses. As known, the removal of Cl species deposited on Al_2O_3 can be considered to be rate-controlling step because of the strong adsorption of Cl species [28]. The reaction of chloro-organics with catalysts Al_2O_3 was also described in the literature concerning the preparation of highly acidic chlorinated alumina catalysts. Chlorination was successfully performed by the reaction of chlorinated alkanes and alkenes containing at least two chlorine atoms.

Several chlorinated alkanes and alkenes can be considered to be less reactive in chlorinating Al_2O_3 [28,29]. The chlorine adsorbed over alumina, as reported by Muddada et al. [30,31], reduced the amount and the acidic strength of the Lewis sites, saturating the coordinate vacancies of Al^{3+} by the formation of Al-Cl species. Higher deactivation rate of $4Ba/Al_2O_3$ can be ascribed to stronger adsorption of HCl on basic sites. As reported in our previous work, the removal of Cl species from catalyst surface can be promoted in the presence of water through providing hydrogen atoms [27]. In this work, the deactivation of Al_2O_3 can not be inhibited by adding water at 350 ^{o}C (Fig. S3), although water promotes the activity of the fresh catalysts at low temperature to some extent (Fig. S4). XPS and EDS analyses showed that Cl deposition on the surface of the used Al_2O_3 and $4Ba/Al_2O_3$ on stream of wet feed at 350 ^{o}C decreases by 50% or more. In the case of the reaction of dichloromethane with water, the balance of a small amount of Cl adsorbed on Al_2O_3 catalyst can be maintained and the activity become constant at 300 ^{o}C [27]. Obviously, the deactivation of Al_2O_3 on wet stream at 350 ^{o}C should be caused only by carbon deposition (Fig. S3). When Al_2O_3 and $4Ba/Al_2O_3$ became deactivated during the stability test, with the addition of 5% O_2 (Fig. 9), the activity of the catalysts can restore almost to the level obtained on the fresh catalysts at 400 ^{o}C. TG-MS confirmed that the removal of black carbon deposited on the surface of catalysts in the presence of oxygen occurred at 430 ^{o}C. In fact, the addition of oxygen, the activity of the dehydrochlorination over Al_2O_3 can not restore completely at 350 ^{o}C (Fig. S5). Here, the removal of Cl species as HCl from the surface of catalysts was promoted by water produced from the oxidation of a small amount of 1,2-DCE.

In the dry and oxygen-free feed, the selectivity of VC increases gradually with the deactivation of Al_2O_3 and reaches 96% at the conversion of 50%, due to the decrease in strong acidic sites through carbon deposition. However, with the removal of carbon from the strong acidic sites in the feed containing oxygen, the dehydrochlorination of VC becomes significant, and the selectivity for VC finally decreases to about 65%. This phenomenon indicates that the strong acidic sites on which black carbon deposits are responsible for the second dehydrochlorination. It is interesting to find that for $4Ba/Al_2O_3$, the selectivity for VC maintains 90% during the stability test (at least 80 h) and almost zero amount of ethyne was detected. $4\%Ba/Al_2O_3$ in particular was tested in the feed containing 5% oxygen for another 80 h at 400 ^oC with the conversion as high as 90-92% and the selectivity for VC as high as 88-90%, respectively (SI). This result is really different from those obtained previously, in which catalytic cracking at 300-400°C on pumice (SiO_2, Al_2O_3, alkalis) or on charcoal, impregnated with $BaCl_2$ or $ZnCl_2$ has not found more widespread application due to the limited life of the catalysts of about 10 h and VC can be further oxychlorinated to ethyl trichloride and further transformed in the presence of oxygen [31]. To our best knowledge, the catalysts used for dehdrochlorination of chlorinated linear paraffins were acidic catalysts, such as silicates and zeolites [1,3,32,33]. Similar results were found in the dehydrochlorination of 1,2-dichloropropane over silica-alumina catalysts where 20% selectivity for allyl chloride and 10 h stability were available [34]. The theoretic and experimental studies showed that the addition of Ba species can cover strong acidic sites of Al_2O_3 [16]. It provided an opportunity to develop a new pathway of 1,2-DCE dehdrochlorination over the catalysts with strong basicity and weak acidity. The synergy of strong base and weak acid is critical to insure good performance of $4Ba/Al_2O_3$. Carbon balance can reach 95% or higher. CO can be detected in effluent due to the oxidation of 1,2-DCE. Inorganic Cl species leave from the reactor as HCl but not as Cl_2. In fact, significant Deacon reaction ($HCl + O_2 \rightarrow Cl_2 + H_2O$) occurs at 700 ^{o}C or higher over Al_2O_3 [35].

In order to understand high selectivity for VC in the presence of oxygen, the oxidation of VC over Al_2O_3 and $4Ba/Al_2O_3$ was conducted. The activity of Al_2O_3 and $4Ba/Al_2O_3$ for VC oxidation is poor, and the conversion reaches 56% and 20% until 350 ^{o}C (Fig. S6). Moreover, the addition of 1,2-DCE can retard the conversion of VC, indicating that 1,2-DCE is more favorable for adsorption on active sites. High selectivity for VC and stable activity over $4Ba/Al_2O_3$ in the presence of oxygen results from its high activity for dehydrochlorination of 1,2-DCE and low activity for the second dehydrochlorination and VC oxidation.

3.2.3 The effect of space velocity

The effect of space velocities on DCE dehydrochlorination over Al_2O_3 and $4Ba/Al_2O_3$ was investigated at 275, 290 and 305 ^{o}C within the space velocities of 30000- 90000 mL g^{-1} h^{-1}. The results (Fig. 10 and Fig. S7) show that the increase in space velocities does not decrease the rate (based on the mol number of 1,2-DCE converted per second per square meter), not as expected. The highest reaction rate was obtained at 60,000 mL g^{-1} h^{-1} and the rates at 30000 and 90000 mL g^{-1} h^{-1} are almost equal. This anomalous datum is associated with the promotion of the removal of Cl species produced during reaction by higher linear rate of feed in the reaction bed, implying that at lower feed rate, HCl desorbed from the surface can go back to the surface. Guido Busca observed this anomalous phenomenon in dehydration of ethanol over Al_2O_3 containing more chlorine impurities [14].

3.3 In situ FTIR spectra

3.3.1 Al_2O_3

FTIR spectra collected at different temperatures during the treatment of the synthesized Al_2O_3 with the reaction feed of 1000 ppm 1,2-DCE in Ar for 1 h after the treatment in Ar at 550 ^{o}C is shown in Fig. 11. The adsorption of 1,2-DCE on Al_2O_3 has been studied between RT and 400 ^{o}C. The spectra was recorded in the absence of gas phase 1,2-DCE unless stated otherwise. It can been seen that at RT, intense bands at 2845 and 2945 cm^{-1} and a weak band at 3040 cm^{-1} (difficult to observe, due to a low signal–noise ratio) are observed, indicating that several types of C–H bonds are present. Raising temperature, the peaks shift to high wavenumbers, 2899 and 2966 cm^{-1} at 200 ^{o}C, indicating the modification of chemical environment. In the section of hydroxyl group, spectra exhibited negative bands in the 3788-3637 cm^{-1} range, which usually are assigned to strong surface hydroxyl groups, along with a weak positive band between 3630-3581 cm^{-1} (centered at approximately 3608 cm^{-1}). These spectra suggest that the Al_2O_3 surface hydroxyl groups interact with 1,2-DCE molecules during adsorption, leading to the formation of weaker hydrogen-bonded OHs [36,37]. After progressive heating in the range of 100–400 ^{o}C, the negative bands in the

3788-3637 cm^{-1} range become strong with temperature in parallel to the increase in the bands due to chlorinated ethoxy groups. Indeed, at RT, 1,2-DCE can react with surface hydroxyl groups. Vigué et al. [38] assumed that the reactivity of alumina surfaces toward halogenated molecules highly suggested that the substitution of surface OH groups by halogenide ions should be easier for the most basic OH groups, corresponding to monocoordinated hydroxyl groups. Consequently, the disappearance of the bands in the 3788-3637 cm^{-1} corresponds to the formation of Al-Cl bonds. In the frequency range between 1800 and 1000 cm^{-1}, weak bands at 1160 and 1194 cm^{-1} corresponding to chlorinated ethoxy are observed within experimental temperature, which shift to higher values, compared with that for CH_3-CH_2O-(1075 and 1116 cm^{-1}) [39]. Previous investigations proposed that the first step in the catalytic oxidation of chlorinated methane over Al_2O_3 catalysts was a nucleophilic substitution [40]. During the nucleophilic substitution, the chlorine atom was abstracted and replaced by oxygen species, forming surface methoxy species and gas HCl [40]. It can be expected that the formation of chlorinated ethoxy species on Al_2O_3, as the first step of dehydrochlorination, is a synergistic effect of nucleophilic attack by basic surface hydroxyl group and the abstraction of Cl atom by acidic Al^{3+} site. While the maxima at 1462 cm^{-1} (δ_{as} C-H of $CClH_2$) and 1400 cm^{-1} (δ_{sym} $CClH_2$) are due to deformation modes of the $CClH_2$ group to which the CH_2 scissoring mode is superimposed. Compared with the case of CH_3, these C-H bands shift to high values slightly, probably due to substitution of Cl for hydrogen. It is interesting to note that, at low temperature of a region from RT to 200 ^{o}C, the absorption band centered at 1647-1665 cm^{-1} is predominant, accompanied by the appearance of two broad strong bands centered at 1409 and 1310 cm^{-1}. Three bands were attributed to a surface enolic species, as similar those bands that were observed on Al_2O_3 during the adsorption of CH_3CHO (not shown). One evidence is that the IR spectra of syn-vinyl alcohol (CH_2=CHOH) in gas phase, show strong absorption band between 1644 and 1648 cm^{-1}, which are accompanied by two bands at 1409-1412 and 1300-1326 cm^{-1} [41,42]. The IR spectrum of adsorbed catechol on a TiO_2 colloid also gives a similar band at 1620 cm^{-1} [43]. Their common characteristic is an enolic structure. On the other hand, a band at 1605 cm^{-1} grows substantially with temperature on stream. Dreoni et al. [44] assigned a strong band observed at 1598 cm^{-1} during adsorption of cyclohexanone on silica at 200 ^{o}C to a C=C stretching vibration. Furthermore, these authors also assigned bands at 3075 and 3045 cm^{-1} to unsaturated =CH– bond stretchings. Indeed, a similar band at 3040 cm^{-1} is also observed in our case during the adsorption of 1,2-DCE and can be assigned to such a vibration mode. Additional bands in the same region at 2939 and 2867 cm^{-1} correspond to C=C and –CH– bonds and are also the present in the spectra of adsorbed 1,2-DCE. The presence of C=C and –CH– bonds further verifies the formation of the enolic form [44]. The bands at 1386, 1268 and 1605 cm^{-1} (assigned to δCH_2, ρCH and γC=C of VC) become significant until 250 ^{o}C, where the conversion to VC in paralleled kinetic reaction is significant. At the same time, there appear new bands at 1680 and 1730 cm^{-1}, ascribed to –C=O group. Generally, an adsorbed acetaldehyde was corresponding to a coordination to a Lewis acid, R–CH=O-Al^{3+} [4]. In fact, -CHO was detected in TPSR as M/Z=29, and in paralleled kinetic reaction, a significant amount of aldehyde in effluent can be observed. Chintawar et al. observed for the adsorption of vinyl chloride on a chromium exchanged zeolite Y a band at 1678 cm^{-1} and assigned this band to an adsorbed aldehyde or ketone [40]. Zhou observed the formation of aldehyde during the decomposition of 1,2-DCE at 260~360 °C [45]. VC can readily be protonated in the presence of acid catalysts, like $AlCl_3$, in the presence of OH surface species into a stable reactive carbonium ion which then was attacked by a nucleophilic oxygen species (basic site of alumina or adsorbed water), leading to the CH_3-CHCl-O species, which would readily decompose to form acetaldehyde and leaving a chloride ion on the surface. Moreover, there appear new bands at 1338~1356 and 1565 cm^{-1} (assigned to carbonate bidentate), 1268, 1425 and 1538 cm^{-1} (asymmetric stretching vibration of carboxylates with the acetate type) [40,46-48], and at 1470 and 1356 cm^{-1} (monodentate bonded carbonates) [49] at 250 °C or higher, probably due to the presence of surface oxygen species, such as basic hydroxyl group.

3.3.2. 4Ba/Al_2O_3

For 4Ba/Al_2O_3, the bands of ascribed to 1,2-DCE adsorption appear at 2880 and 2965 cm^{-1} (several types C–H bond, Fig. 12), consistent with that observed on Al_2O_3. However, the band intensity seems much weak. Additionally, the band splits in various range section can be observed, suggesting 1,2-DCE adsorption on two different types of sites associated with BaO and Al_2O_3. At the same time, the bands resulted from oxidized surface species as carbonate bidentate (appearing at 1338~1356 and 1565 cm^{-1}), asymmetric stretching vibration of carboxylates with the acetate type (appearing at 1268, 1425 and 1540 cm^{-1}) and monodentate bonded carbonates (appearing at 1473 and 1356 cm^{-1}) become much stronger at 200 ^{o}C. Oxidation products were seen in the absence of gas-phase oxygen, indicating involvement of surface oxygen in this process. As reported, formaldehyde and formic acid were detected on spectra during the adsorption of dichloro-methane on Al_2O_3 [50]. In fact, their formation was resulted from the nucleophlical attacks by surface hydroxyl group or oxygen species to dichloro-methane to produce methoxy species and the following disproportionation. Probably, these oxidized products in this work are related to incorporation of hydroxyl group and basic oxygen species into the adsorbed 1,2-DCE molecules. A small amount of alkali metal was known to make alumina basic [51]. The addition of Ba increases inevitably strong basic oxygen species. As expected, there are more oxidized products on $4Ba/Al_2O_3$. It should be noted that the band corresponding to carbonyl group of aldehyde is not observed on $4Ba/Al_2O_3$, while aldehyde was detected in effluent with a significant amount. Based on the fact that $4Ba/Al_2O_3$ possesses less strong acid sites, it can be concluded that aldehyde produced mainly adsorbs on strong acid sites as R–CH=O-Al^{3+}. The same phenomenon is observed on Al_2O_3-C with less strong acid sites (Fig. S8), where the carbonate bidentate, carboxylates with the acetate type and monodentate bonded carbonates can not be observed within experimental temperature. These results imply that the oxidation involving surface oxygen species on Al_2O_3-C is weak, probably relating to without strong basic sites or strong acid sites.

Based on these experiments it was postulated that the first step in the interaction of 1,2-DCE with Lewis acid sites occurs and the adsorbed 1,2-DCE can be attacked nucleophlically by oxygen to form chlorinated ethoxy intermediate through the removal of chlorine atom. The formation of VC occurs through transfer of proton and rearrangement of chlorinated ethoxy. The rearrangement of ethoxy intermediate was considered to be an indispensable step in the dehydration of ethanol on pure Al_2O_3 [14]. At the same time, VC adsorbed on two sites, a pair of acidic-basic sites can be converted into carbonyl species which may or may not contain chlorine, and stabilized by resonance (an enolic structure). And with the destruction of VC, the formation of aldehyde was proposed. A following oxygen attack on the carbonyl compound results in the formation of carboxylate and carbonate species [40]. On the other hand, on strong acidic sites, chlorine atom of VC can be abstracted with the transfer of proton, and ethyne formed. In order to obtain deep insights into this reaction at a molecular level, a mechanism over Al_2O_3 consisting of three elementary steps is schematized (Fig. 13): (1) the formation of 1,2-DCE adsorption complex during the interaction of 1,2-DCE with Lewis acid sites; (2) chlorine abstraction by nucleophilic oxygen (surface hydroxyl groups) to form chlorinated ethoxy intermediate; (3) dehydroxylation through rearrangement to form VC. Other side reactions include: (1) the attack of basic oxygen species to VC; (2) the formation of oxygenate species, such as aldehedy, carbonate bidentate, monodentate and partially oxidized surface species such as enolic species, acetates, carboxylates of the acetate type; (3) the formation of ethyne through the interaction of VC with strong Lewis acid sites, such as tetrahedral Al^{3+} ions at high temperature.

4. Conclusion

Bimodal mesoporous Al_2O_3 was prepared using polyethyleneglycol (PEG 20000) and cetyl trimethyl ammonium bromide as template. Ba/Al_2O_3 catalysts with Ba loading of 1~10 wt% obtained by incipient wetness were characterized by XRD, BET and porosity measurements, and Py-FT-IR, and used in catalytic dehydrochlorination of 1,2-DCE. The results showed that Ba species was highly dispersed on Al_2O_3 probably as monomeric or dimmeric BaO. The number of surface tetrahedral Al^{3+} ions decreases with Ba loading, which corresponds to the decrease in strong acid sites. In the catalytic dehydrochlorination of 1,2-DCE, Ba/Al_2O_3 catalysts present high activity, of which Al_2O_3 is most active with 95% conversion at 325 ^{o}C. The products are composed of VC, aldehyde, ethyne and butene. The formation of aldehyde occurs at low 1,2-DCE conversion (at low temperature) and butane appears at higher temperature with low selectivity (below 1%). For Al_2O_3, the selectivity for VC reaches 95% at 350 ^{o}C, However, at higher temperature, the selectivity decreases quickly and is only 40% at 425 ^{o}C, which is related to a significant formation of ethyne. The addition of Ba really promotes the selectivity for VC at high temperature through the decrease in strong acidic sites which are favorable for the second dehydrochlorination. Al_2O_3 and $4Ba/Al_2O_3$ deactivate heavily on the stream within 20 h at 400 ^{o}C, due to the deposition of carbon and chlorine species. The presence of oxygen with a small amount can effectively promote the stability, in which 90% conversion and 90% selectivity for VC on $4Ba/Al_2O_3$, are available. *In situ* FTIR showed that the first step in the interaction of 1,2-DCE with Lewis acid sites occurs and the adsorbed 1,2-DCE can be attacked nucleophlically by oxygen to form chlorinated ethoxy intermediate through the removal of chlorine atom. The formation of VC occurs through transfer of proton and rearrangement of chlorinated ethoxy. Different types of partially oxidized products, including the enolic form of aldehyde-type intermediate, were observed because of the attack to VC by hydroxyl or basic oxygen species existing on the surface of Al_2O_3 or $4Ba/Al_2O_3$ catalysts.

Acknowledgments

This research was supported by Development Program for National Natural Science Foundation of China (Nos. 21277047, 21477036 and 21307033).

Reference

[1] A. S. Shalygin, L. M. Koval, L. V. Malysheva, N. S. Kotsarenko and E. A. Paukshtis, *Chem. Sust. Dev.*, 2009, **17**, 417–422.

[2] A. Lakshmanan, W. C. Rooney and L. T. Biegler, *Comput. Chem. Eng.*, 1999, **23**, 479–495.

[3] I. Mochida, A. Uchino, H. Fujitsu and K. Takeshita, *J. Catal.*, 1978, **51**, 72–79.

[4] M. M. R. Feijen-Jeurissen, J. J. Jorna, B. E. Nieuwenhuys, G. Sinquin, C. Petit and J. P. Hindermann, *Catal. Today.*, 1999, **54**, 65–79.

[5] G. Busca, *Catal. Today.*, 2014, **226**, 2–13.

[6] B. C. Lippens and J. H. de Boer, *Acta Crystallogr.*, 1964, **17**, 1312–1321.

[7] A. R. Ferreira, M. J. F. Martins, E. Konstantinova, R. B. Capaz, W. F. Souza, S. S. X. Chiaro and A. A. Laitão, *J. Solid State Chem.*, 2011, **184**, 1105–1111.

[8] R. S. Zhou and R. L. Snyder, *Acta Crystallogr*. B, 1991, **47**, 617–630.

[9] J. H. Kwak, J. Z. Hu, D. H. Kim, J. Szanyi and C. H.F. Peden, *J. Catal.*, 2007, **251**, 189–194.

[10] G. Paglia, A. L. Rohl, C. E. Buckley and J. D. Gale, *Phys. Rev. B*, 2005, **71**, 224115–224116.

[11] L. Smrcok, V. Langer and J. Krestan, *Acta Crystallogr. C.*, 2006, **62**, 83–84.

[12] M. Digne, P. Sautet, P. Raybaud, P. Euzen and H. Toulhoat, *J. Catal.*, 2004, **226**, 54–68.

[13] M. Digne, P. Sautet, P. Raybaud, P. Euzen and H. Toulhoat, *J. Catal.*, 2002, **211**, 1–5.

[14] T. K. Phung, A. Lagazzo, M. Á. R. Crespo, V. S. Escribano and G. Busca, *J. Catal.*, 2014, **311**, 102–113.

[15] P. Bai, P. P. Wu and Z. F. Yan. *Micropor. Mesopor. Mater.*, 2009, **118**, 288–295.

[16] H. Kwak, D. Mei, C. W. Yi, D. H. Kim, C. H. F. Peden, L. F. Allard and J. Szanyi, *J. Catal.*, 2009, **261**, 17–22.

[17] J. H. Kwak, Hu JZ, D. Mei, C. W. Yi, D. H. Kim, C. H. F. Peden, L. F. Allard and J. Szanyi, *Science.*, 2009, **325**, 1670–1673.

[18] H. Knözinger and P. Ratnasamy, *Catal. Rev.: Sci. Eng.*, 1978, **17**, 31–70.

[19] C. Morterra and G. Magnacca, *Catal. Today.*, 1996, **27**, 497–532.

[20] X. Liu and R.E. Truitt, *J. Am. Chem. Soc.*, 1997, **119**, 9856–9860.

[21] D. T. Lundie, A. R. McInroy, R. Marshall, J. M. Winfield, P. Jones, C. C. Dudman, S. F. Parker, C. Mitchell and D. Lennon, *J. Phys. Chem. B*, 2005, **109**, 11592–11601.

[22] Silvia Bordiga, Carlo Lamberti, Francesca Bonino, Arnaud Travertd and Frederic Thibault-Starzyk, *Chem. Soc. Rev.*, 2015, **44**, 7262-7341.

[23] G. Busca, *Chem. Rev.*, 2010, **110**, 2217–2249.

[24] A.E. Kulikova and E.N. Zilberman, *Russian Chem. Rev.*, 1971, **40**, 256–271.

[25] G. C. Bond and N. Sadeghi, *J. Appl. Chem. Biotechnol.*, 1975, **25**, 241–248.

[26] P. S. Chintawar and H. L. Greene, *Appl. Catal. B, Environ.*, 1997, **13**, 81–92.

[27] L. Ran, Z. Qin, Z. Y. Wang, X. Y. Wang and Q. G. Dai, *Catal. Commun.*, 2013, **37**, 5–8.

[28] G. Clet, J. M. Goupil and D. Cornet, *Bull. Soc. Chim. Fr.*, 1997, **134**, 223–233.

[29] A. G. Goble and P. A. Lawrance, in: Proc. 3rd Int. Cong. Catal.,vol. I, North Holland, Amsterdam, 1964, 320.

[30] N.B. Muddada, U. Olsbye, T. Fuglerud, S. Vidotto, A. Marsella, S. Bordiga, D. Gianolio, G. Leofanti and C. Lamberti, *J. Catal.*, 2011, **284**, 236–246.

[31] G. Leofanti, A. Marsella, B. Cremaschi, M. Garilli, A. Zecchina, G. Spoto, S. Bordiga, P. Fisicaro, G. Berlier, C. Prestipino, G. Casali and C. Lamberti, *J. Catal.*, 2001, **202**, 279-295.

[32] K. Weissermel and H. J. Arpe, *Industrial Organic Chemistry*, 3rd ed.; VCH: Weinheim, Germany, 1997; p 219;

[33] E. L., Dreher, *Ullmann's Encyclopedia of Industrial Chemistry*; VCH: Weinheim, Germany, 1986; A6, p 289.

[34] C. Pistarino, E. Finocchio, M. A. Larrubia, B. Serra, S. Braggio, G. Busca, *Ind. Eng. Chem. Res.*, 2001, **40**, 3262-3269

[35] M. W. M. Hisham and S. W. Benson, *J. Phys. Chem.*, 1995, **99**, 6194–6198.

[36] D. Carmello, E. Finocchio, A. Marsella, B. Cremaschi, G. Leofanti, M. Padovan and G. Busca, *J. Catal.*, 2000, **191**, 354–363.

[37] B. H. Aristizábal, C. M. de Correa, A. I. Serykh, C. E. Hetrick and M. D. Amiridis, *Micropor. Mesopor. Mat.*, 2008, **112**, 432–440.

[38] H. Vigué, P. Quintard, T. Merle-Méjean and V. Lorenzelli, *J. Eur. Ceram. Soc.*, 1998, **18**, 305–309.

[39] A. Starczewska, R. Wrzalik, M. Nowak, P. Szperlich, Ł. Bober, J. Szala, D. Stroz and D.Czechowicz, *Infrared Phys. Tech.*, 2008, **51**, 307–315.

[40] P. S. Chintawar and H. L. Greene, *J. Catal.*, 1997, **165**, 12–21.

[41] M. Mikami, I. Nakagawa and T. Shimanouchi, *Spectrochim. Acta.*, 1967, **23A**, 1037–1053.

[42] M. Rodler, C. E. Blom and A. Bauder, *J. Am. Chem. Soc.*, 1984, **106**, 4029–4035.

[43] T. Rajh, L. X. Chen, K. Lukas, T. Liu, M. C. Thurnauer and D. M. Tiede, *J. Phys. Chem. B*, 2002, **106**, 10543–10552.

[44] D. P. Dreoni, D. Pinelli, F. Trifiro, G. Busca and V. Lorenzelli, *J. Mol. Catal.*, 1992, **71**, 111–127.

[45] Q.Q. Huang, Z.H. Meng and R.X. Zhou, *Appl. Catal. B: Environ.*, 2012, **115-116**, 179-189.

[46] S. Krishnamoorthy, J. A. Rivas and M. D. Amiridis, *J. Catal.*, 2000, **193**, 264–272.

[47] V. E. Suprunov and A. A. Ivanov, *React. Kinet. Catal. Lett.*, 1987, **33**, 75–80.

[48] V. S. Escribano, G. Busca and V. Lorenzelli, *J. Phys. Chem.*, 1990, **94**, 8939–8945.

[49] M. L. Hair, Infrared Spectroscopy in Surface Chemistry, Marcel Dekker, New York, 1967, p. 205–208.

[50] I. Maupin, L. Pinard, J. Mijoin and P. Magnoux, *J. Catal.*, 2012, **291**, 104–109.

[51] H. Pines and W. O. Haag, *J. Am. Chem. Soc.*, 1960, **82**, 2471–2483.

Table 1. Physicochemical properties of Al_2O_3 and Ba/Al_2O_3 with various Ba loadings

Sample	S_{BET} (m^2g^{-1})	V_{pore} (cm^3g^{-1})	D_{pore} (nm)	Total acidity (mmol /g cat)[a]		Activity (°C)	
				weak acid	strong acid	T_{50}	T_{95}
Al_2O_3	330	0.434	3 / 7	0.149	0.082	308	355
$1Ba/Al_2O_3$	301	0.366	3 / 6	0.162	0.100	315	360
$2Ba/Al_2O_3$	321	0.383	3 / 6	0.173	0.070	329	381
$4Ba/Al_2O_3$	334	0.390	2.7/5	0.108	0.060	338	404
$10Ba/Al_2O_3$	304	0.302	2.5/ 5	0.101	0.052	392	472
Al_2O_3-C	118	0.253	6	0.088	0.043	386	441

[a] Determination by NH_3-TPD tests.

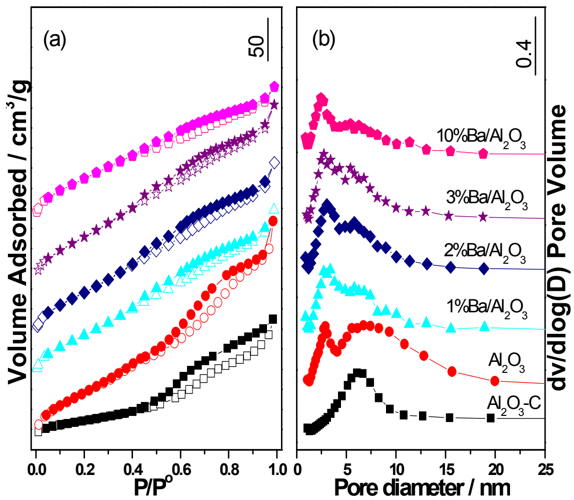

Fig. 1. N_2 sorption isotherms (a) and pore size distribution (b) of Al_2O_3, Ba/Al_2O_3 and Al_2O_3-C samples.

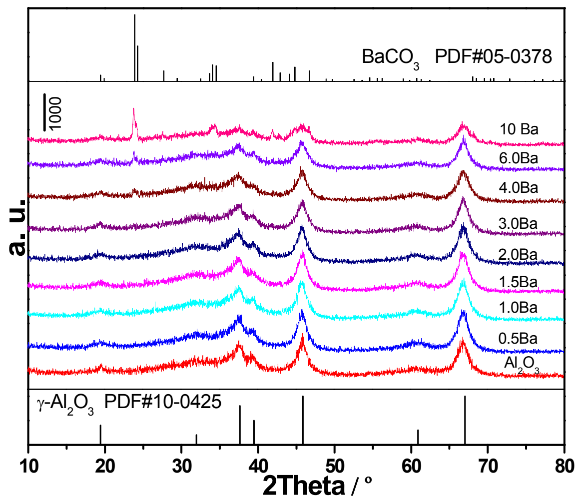

Fig. 2. XRD patterns of Al_2O_3 and Ba/Al_2O_3 samples with various Ba loadings.

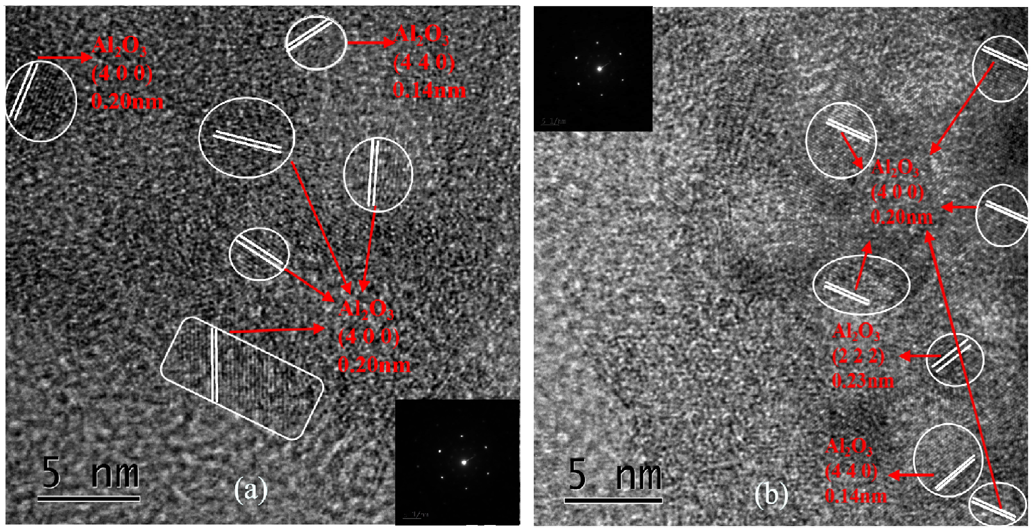

Fig. 3. HRTEM and SAED (insert) images of Al_2O_3 (a) and $4Ba/Al_2O_3$ samples (b).

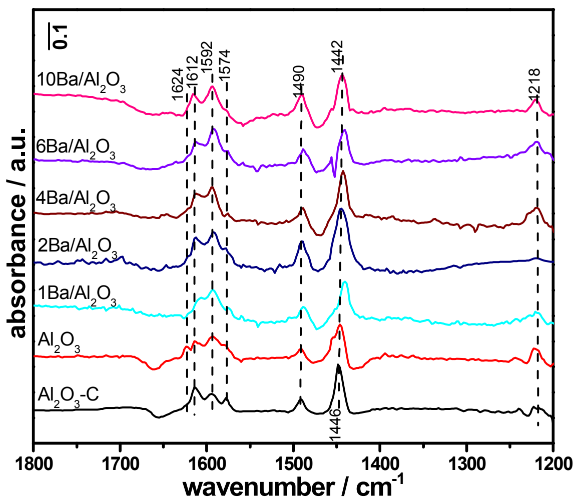

Fig. 4. Py-FT-IR spectra of Al_2O_3 and Ba/Al_2O_3 samples at 200°C.

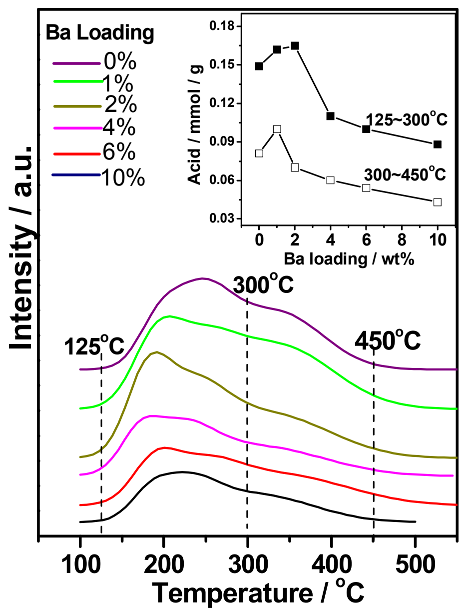

Fig. 5. NH_3-TPD profiles and the amount of NH_3 desorbed (insert) at 125-300 °C and 300-450 °C from Al_2O_3 and Ba/Al_2O_3 samples with various Ba loadings.

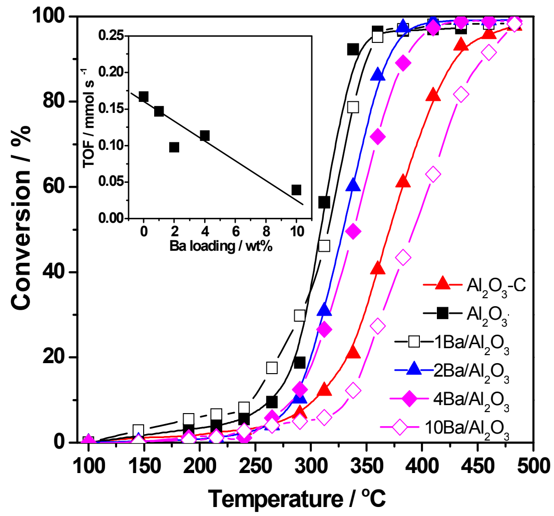

Fig. 6. The conversion curves of 1,2-DCE and TOF (insert, based on the mole number converted 1,2-DCE at 300 °C per second per acidic site) over different catalysts; reaction gas: 1000 ppm 1,2-DCE and Ar balance; SV=30,000 mL g^{-1} h^{-1}.

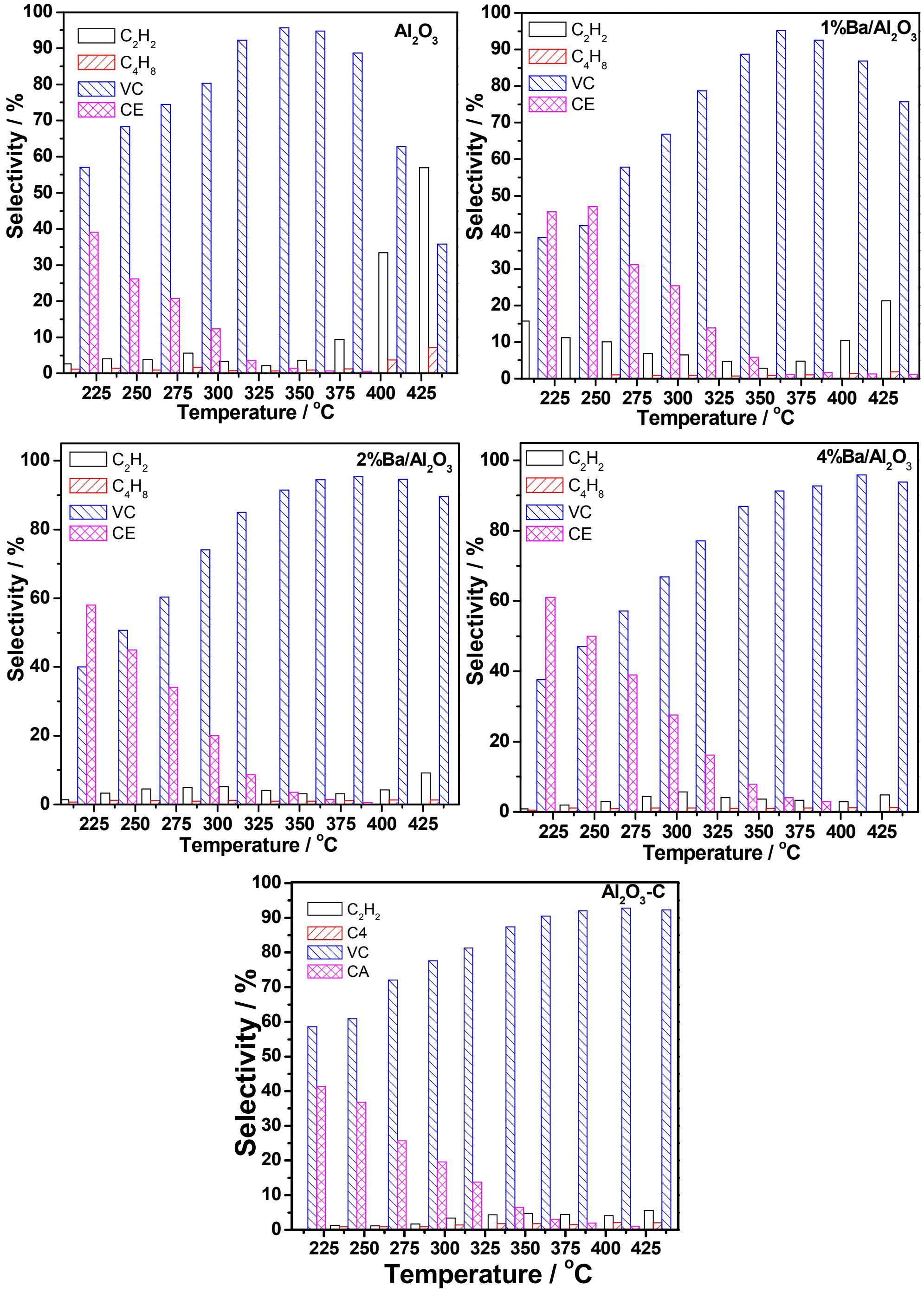

Fig. 7. The distribution of products obtained in the reactions under conditions as same as described in Fig. 6.

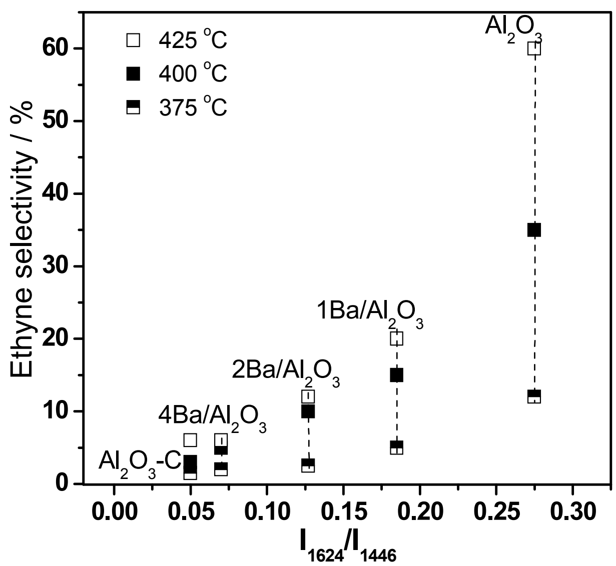

Fig. 8. Correlation of Ethyne selectivity with I_{1624}/I_{1448} for catalysts at various temperature; reaction gas: 1000 ppm 1,2-DCE and Ar balance; SV=30,000 mL g^{-1} h^{-1}.

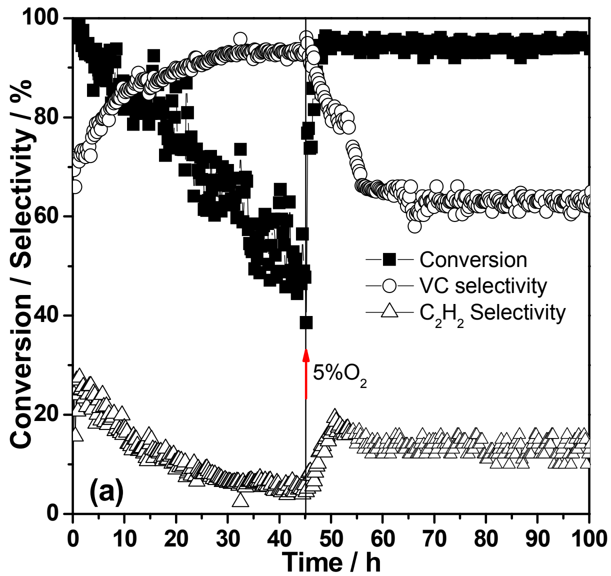

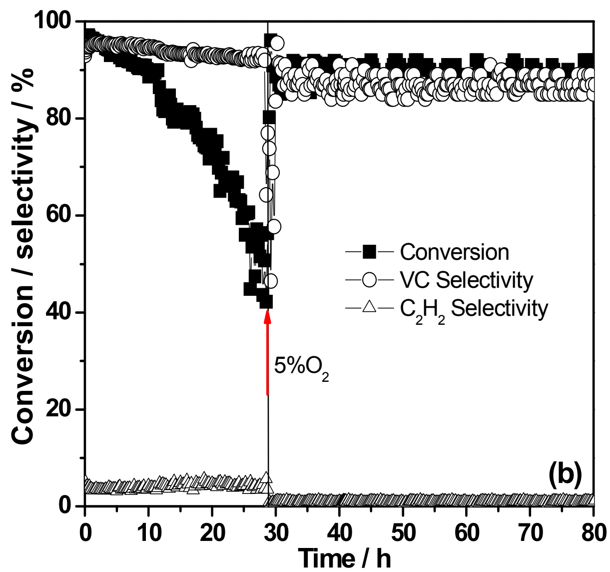

Fig. 9. The stability on the feed streams at 400 °C of Al_2O_3 (a) and 4Ba/Al_2O_3 (b) catalysts; reaction gas: 1000 ppm 1,2-DCE and Ar balance; SV=30,000 SV=30,000 mL g^{-1} h^{-1}.

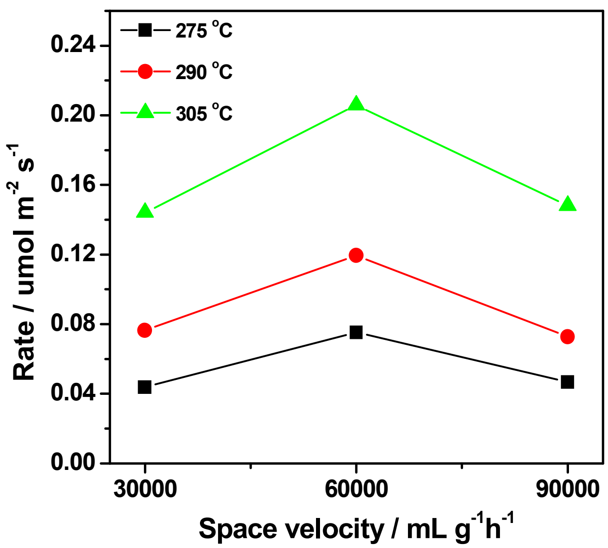

Fig. 10. Relationship between the space velocities and rates of 1,2-DCE dehydrochlorination over Al_2O_3 catalyst.

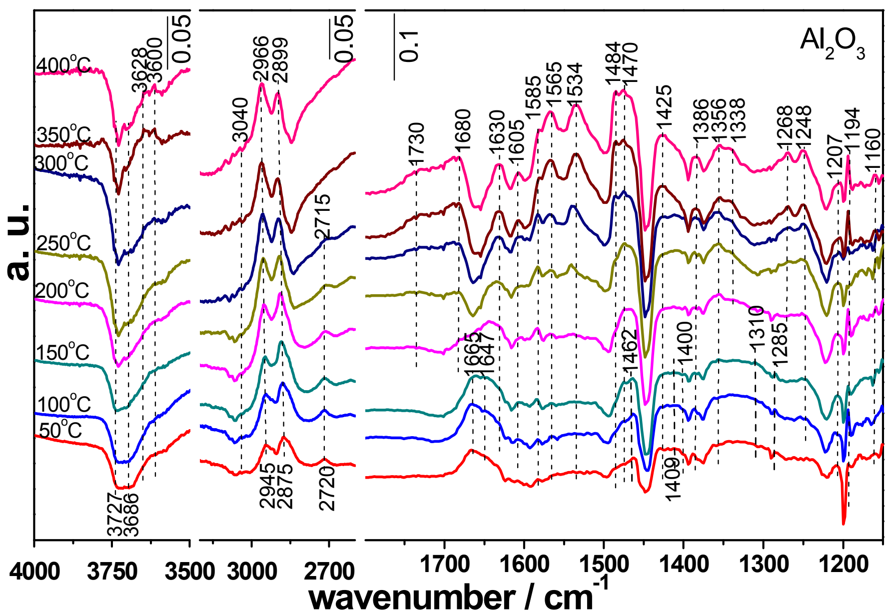

Fig. 11. *In situ* FTIR spectra in 1100-4000 cm^{-1} region for Al_2O_3 in a 1000 ppm 1,2-DCB/Ar stream from 50 to 400 °C after the treatment in Ar at 550 °C.

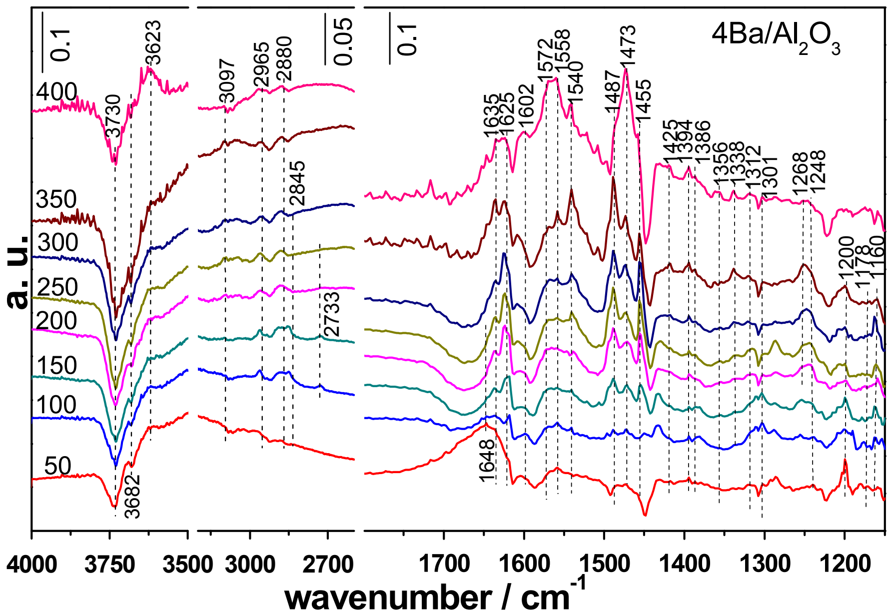

Fig. 12. *In situ* FTIR spectra in 1100-4000 cm^{-1} region for $4Ba/Al_2O_3$ in a 1000 ppm 1,2-DCB/Ar stream from 50 to 400 ^{o}C after the treatment in Ar at 550 ^{o}C.

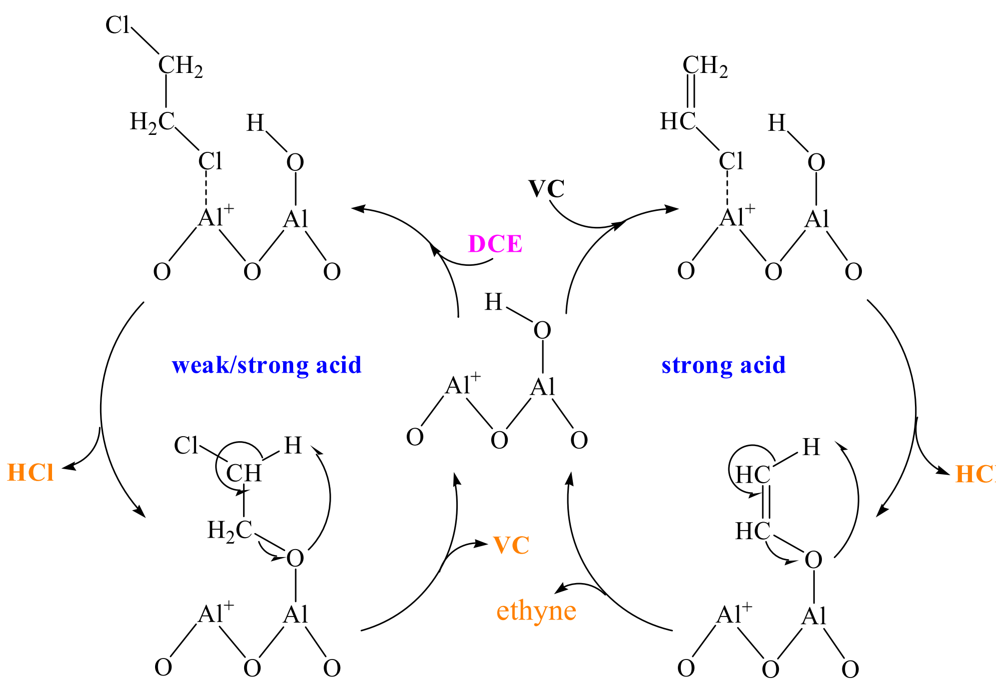

Fig. 13. Reaction pathway for 1,2-DCE dehydrochlorination over γ-alumina.